Nuclear Physics A512 (1990) 253-274
North-Holland

LARGE-AMPLITUDE MOTION IN SUPERFLUID FERMI DROPLETS

F. BARRANCO

Departmento de Fisica Aplicada, ETSII, Universidad de Sevilla, Avda. Reina Mercedes, Sevilla, Spain

G.F. BERTSCH

National Superconducting Cyclotron Laboratory and Department of Physics-Astronomy, Michigan State University, East Lansing, MI 48824, USA

R.A. BROGLIA and E. VIGEZZI

Dipartimento di Fisica, Universita di Milano, and INFN Sez. Milano, 20133 Milano, Italy
and
The Niels Bohr Institute, University of Copenhagen, DK-2100 Copenhagen Ø, Denmark

Received 16 October 1989

Abstract: Large-amplitude motion in the nuclear shape degrees of freedom are described by superfluidity within a finite-basis model space. The technique allows an inertial parameter to be constructed for arbitrary shape changes. Application is made to alpha- and heavy-particle radioactivity.

1. Introduction

Paradoxically, the theory of large-amplitude collective motion in nuclei is both well-developed and poorly understood. Potential energy surfaces describing the nuclear shape degrees of freedom can be constructed using Hartree-Fock theory [1]) or simplifications thereof, such as the Strutinsky method [2-4]). To calculate dynamics, one also needs inertial parameters corresponding to these degrees of freedom. The standard technique, cranked mean field theory, is straightforwad in principle, but the use of continuous collective coordinates obscures the essential discreteness of the Hartree-Fock basis of wave functions. Doubt about the continuum treatment is raised by the behavior of the inertia function, which has large fluctuations associated with specific Hartree-Fock configurations [2]). Furthermore, the obvious choice of the constraining field may lead to too large a value for the cranked inertia [5,6]). Another technique, based on the continuation of time-dependent mean field theory to imagnary time, resolves this problem in principle, but in practice may be too difficult to apply numerically to realistic cases [6,7]).

0375-9474/90/$03.50

This paper is an attempt to construct a model of large-amplitude motions closer to the actual physics of configurational changes. We do not claim that the approach is fundamentally superior to the above methods. Rather, we believe that it is easier to apply effectively to a wide variety of problems [8-11]), because it deals with the relevant aspects of the many-particle wave functions.

In the next section we describe, in general terms, how a model with a discrete basis is applied to situations normally described with a collective coordinate. It is necessary to understand the level density as a function of the coordinate, and the hamiltonian matrix connecting different levels. These topics are discussed in sects. 3 and 4, respectively. The main application of the model is to particle emission. We describe calculations of alpha- and heavy-particle radioactivity in sect. 5. Finally, in sect. 6 we discuss the reliability of the model and the prospects for further applications.

2. Discrete models for large-amplitude motion

We want to describe the wave functions of the nucleus as a linear combination of Hartree-Fock determinants. The details of the Hartree-Fock states will not be discussed; we are interested in the relationships between them that can be established to hold on the average. We consider collective motion along a path in the space of deformations, and describe it in terms of a single coordinate, with the determinants ordered according to the value of that coordinate. To pass from one determinant to another, one must make particle-hole excitations in the starting determinant and alter the single-particle wave function slightly in order to correspond to the new Hartree-Fock field. This picture was introduced by Hill and Wheeler [12]) in an attempt to describe the fission process. We say that two configurations are "neighboring" if there is a high overlap between one and a 2p2h excitation of the other. We assume that the hamiltonian can only connect neighboring configurations. Also, it is clear that configurations of quite different shapes cannot be neighbors.

The simplest model to describe collective motion between two shapes would be to link configurations near these shapes by a chain of neighboring configurations [13]). The chains with lowest energy intermediate states would be particularly favored, and would give the most primitive basis for the active states. Then the equation describing the shape evolution is

$$\begin{bmatrix} \ddots & & & \\ E_{i-1} & v & & \\ v & E_i & v & \\ & v & E_{i+1} & \\ & & & \ddots \end{bmatrix} \begin{pmatrix} \vdots \\ a_{i-1} \\ a_i \\ a_{i+1} \\ \vdots \end{pmatrix} = E_\alpha \begin{pmatrix} \vdots \\ a_{i-1} \\ a_i \\ a_{i+1} \\ \vdots \end{pmatrix}. \tag{2.1}$$

Here E_i is the Hartree-Fock energy of configuration i, and v, taken to be constant, is the off-diagonal matrix element connecting neighboring configurations. The sol-

ution of the hamiltonian problem yields eigenfunctions which are linear combinations of the basis determinantal states ϕ_k

$$\Phi_\alpha = \sum_{k=1}^{n} a_k^\alpha \phi_k . \tag{2.2}$$

The energetics of the process described by (2.2) is sketched in fig. 1, which depicts energy levels as a function of some deformation coordinate. Each energy level is a parabola. The bottom is a Hartree-Fock state of some definite energy E_i, and the other points show how the energy changes when the state is deformed. It is energetically very unfavorable to move any distance along the same state. The large-scale shape changes must then come from the jumps from one state to another.

The determinant ϕ_0 describes the configuration associated with the absolute minimum corresponding to the equilibrium shape of the parent nucleus, while ϕ_n is the Slater determinant associated with the touching configuration of the daughter nuclei (cf. fig. 2).

Before filling in details of the picture, we show how a collective hamiltonian may be derived from a discrete model. A collective hamiltonian would have a Schrödinger equation of the form

$$\left(-\frac{\hbar^2}{2D} \frac{\mathrm{d}^2\Phi(\xi)}{\mathrm{d}\xi^2} + V(\xi) \right) \Phi_\alpha(\xi) = E\Phi_\alpha(\xi) . \tag{2.3}$$

Discretizing this equation on a mesh in ξ, the second derivative operator is replaced

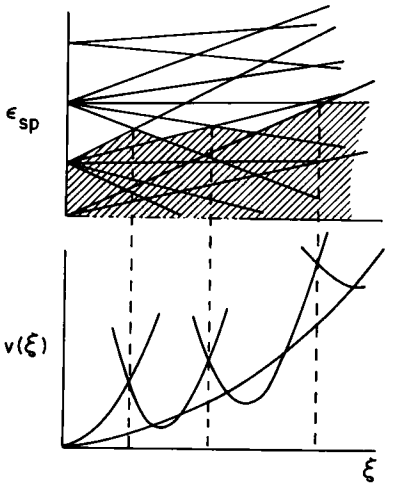

Fig. 1. Schematic representation of the occupancy of the single-particle levels and of the local Hartree-Fock potential energies as a function of the deformation parameter ξ. At $\xi = 0$ the parent nucleus is assumed to be in the spherical ground state. When the nucleus goes away from equilibrium, the single-particle levels split gaining or losing binding energy according to whether the associated orbit is along the deformation or perpendicular to it.

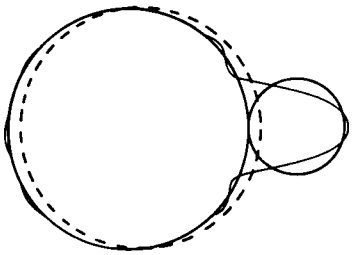

Fig. 2. We illustrate with an example relevant to heavy-particle radioactivity, specifically $^{232}U \rightarrow {}^{21}Ne + {}^{208}Pb$. The initial shape (dashed curve) is that of the uranium nucleus, which is taken to be an ellipsoid with deformation $\beta_2 = 0.225$. The final shape (continuous curve) is that of two spheres corresponding to ^{24}Ne and ^{208}Pb. The separation of the spheres is such that the two half density radii touch. The transformation described in the text carries the initial shape to the one shown by the thin solid line.

by a second difference

$$\frac{d^2\Phi_\alpha(\xi)}{d\xi^2} = \frac{\Phi_\alpha(\xi_{i-1}) + \Phi_\alpha(\xi_{i+1}) - 2\Phi_\alpha(\xi_i)}{(\Delta\xi)^2}. \tag{2.4}$$

The matrix for H is tridiagonal, and from comparison with (2.1) we identify

$$D = -\frac{\hbar^2}{2v}(\Delta\xi)^{-2}, \qquad E_i = V(\xi) + 2v, \tag{2.5}$$

where $\Delta\xi$ is the mesh spacing.

3. State counting

Our first task in the discrete state modelling of collective motion is to determine the average distance between neighboring configurations. This will determine $\Delta\xi$ and the distance scale in large-amplitude motion. We find the distance between states by deforming the nucleus according to the required shape change, making a criterion to determine when the nucleus has reached a new Hartree–Fock configuration.

We first deform the wave function with a single-particle field, $F(\boldsymbol{r})$. The wave function will be transformed to [14])

$$\phi'_k(\boldsymbol{r}) = e^{\nabla F \cdot \nabla}\, \phi_k(\boldsymbol{r}) \approx \phi_k(\boldsymbol{r} + \nabla F). \tag{3.1}$$

In order to make the new state as low in energy as possible, we shall restrict ourselves to incompressible fields, $\nabla^2 F = 0$. Then F may be expressed as

$$F(\boldsymbol{r}) = \sum_\lambda c_\lambda r^\lambda Y_\lambda(\hat{\boldsymbol{r}}). \tag{3.2}$$

The transformation (3.1) alters the momentum distribution in the nucleus. This may be readily seen by examining the Wigner function of the transformed state,

$$f'(\boldsymbol{r},\boldsymbol{p}) = \int \mathrm{e}^{i\boldsymbol{p}\cdot\boldsymbol{s}}\,\phi_k^*(\boldsymbol{r}+\tfrac{1}{2}\boldsymbol{s}+\nabla F(\boldsymbol{r}+\tfrac{1}{2}\boldsymbol{s}))\phi_k(\boldsymbol{r}-\tfrac{1}{2}\boldsymbol{s}+\nabla F(\boldsymbol{r}-\tfrac{1}{2}\boldsymbol{s}))\,\mathrm{d}^3s$$

$$\approx \int \mathrm{e}^{i\boldsymbol{p}\cdot\boldsymbol{s}}\phi_k^*(\boldsymbol{r}+\nabla F+\tfrac{1}{2}\boldsymbol{s}(1+\nabla\nabla F))\phi_k(\boldsymbol{r}+\nabla F-\tfrac{1}{2}\boldsymbol{s}(\mathbb{1}+\nabla\nabla F))\,\mathrm{d}^3s$$

$$\approx f(\boldsymbol{r}+\nabla F,\boldsymbol{p}(1+\nabla\times\boldsymbol{F})^{-1})\,. \tag{3.3}$$

Here $\nabla\times\boldsymbol{F}$ is a second-order tensor in the cartesian variable, and $\mathbb{1}$ the 3×3 unit matrix in the same space. The new shape of the system has been achieved at the cost of a deformed Fermi surface. This gives the system a higher kinetic energy.

A state of lower energy can be constructed by moving the particles above the spherical Fermi surface below. In the classical limit, moving particles in momentum space will not change the density distribution, as long as the volume in momentum space remains constant. Of course, the single-particle basis in the wave function first has to be transformed to a representation with particles above and below the Fermi sphere. This is not always possible. A given particle wave function might be distributed partly above and partly below the Fermi sphere. If there is a nonintegral number of particles above, there is no way a spherical Fermi surface could be restored. Such a necessary condition for restoring a spherical Fermi surface is that the integral of the Wigner function outside the Fermi sphere equals an integer. We assume that this is sufficient, also for the existence of a single-particle representation that allows a new Hartree–Fock minimum to be reached by moving particles between the orbitals.

Since the local density is approximately preserved in the second transformation, the potential energy of the system associated with a short-range interaction will be the same. The kinetic energy is also preserved, because the Fermi surface has been restored to a spherical shape. Thus, the new state will have essentially the same energy as the original state.

Of course, effects associated with the finite range of the interaction and the quantum mechanics of the surface energy remain, which will ultimately produce a liquid drop behavior of the energy function. In addition, there will be shell fluctuation effects associated with imperfections in the sphericity of the Fermi surface.

The general formula for the criterion is that the following integral be equal to an integer,

$$g\int_{|p|>p_F}\frac{\mathrm{d}^3p\,\mathrm{d}^3r}{(2\pi)^3}f'(\boldsymbol{r},\boldsymbol{p}) = n\,. \tag{3.4}$$

Here g represents the spin, and possibly isospin, degeneracy of the single-particle levels. Thus, to deform a heavy nucleus to get to a neighboring configuration with two neutrons moved to a different orbital, we would apply the criterion given by

eq. (3.4) with $n=2$ and $g=2$. On the other hand, for light nuclei like ^{40}Ca, or even more so ^{16}O, spin and isospin symmetry imply that changes in the deformation come about by moving around alpha clusters, requiring $g=4$ and $n=4$ for the nearest low state.

We simplify the integral in eq. (3.4) continuing in the semiclassical spirit. The initial Wigner function is assumed to be sharp-edged, with value 0 or 1. To evaluate the integral over momentum, we need the eigenvalues of the 3×3 matrix $\nabla\times\nabla F$. Calling the eigenvalues F_i, the constant-volume condition is $F_1+F_2+F_3=0$. Also, we assume $F_2=F_3$. Then the momentum integral is reduced using

$$\int \frac{d^3p}{(2\pi)^3}\,\theta(|\boldsymbol{p}(1+\nabla\times\nabla F)^{-1}|-p_F)\theta(p_F-p)$$

$$\approx \frac{2\pi}{(2\pi)^3}p_F^3\int d\cos\nu\,\theta(F_1\cos^2\nu-F_2\sin^2\nu)\theta(-F_1\cos^2\nu-F_2\sin^2\nu)$$

$$=\frac{4\pi}{(2\pi)^3}\tfrac{1}{3}\sqrt{\tfrac{1}{3}}p_F^3F_{11}\,. \tag{3.5a}$$

Now, one can conveniently re-express eq. (3.4) using the semiclassical relation between volume and particle number, $g\,\frac{4}{3}\pi p_F^3/(2\pi)^3\;V=A$, where V is the spatial volume of the system. This is,

$$n=A\int\frac{d^3r}{V}\frac{F_{11}(r)}{\sqrt{3}}=\sqrt{\tfrac{1}{3}}A\langle F_{11}(r)\rangle\,. \tag{3.5b}$$

The formula is very simple for pure quadrupole deformation. Writing $F=\beta_2 r^2 Y_{20}$, we have

$$\nabla\nabla F=\sqrt{\frac{5}{4\pi}}\beta_2\begin{bmatrix}2&0&0\\0&-1&0\\0&0&-1\end{bmatrix}, \tag{3.6}$$

and $F_{11}=2\beta_2\sqrt{5/4\pi}$. Since F_{11} is constant the spatial integration is trivial in eq. (3.4), and we obtain

$$n=\sqrt{\tfrac{1}{3}}A\left(2\beta_2\sqrt{\frac{5}{4\pi}}\right). \tag{3.7}$$

For heavy nuclei, this formula has been demonstrated to be accurate to about 10% counting the level crossing over large intervals of deformation. It is also surprisingly accurate for finding the deformation of low deformed states in light nuclei*.

For more general F, reduction of the integral is not so simple and it has to be evaluated numerically. For reference we quote in appendix A the matrix $\nabla\times\nabla F$ for multipoles up to $L=4$.

* The gravity between n and β has been found to hold in light nuclei for values up to $n=8$ [ref. [15])].

A technical problem that arises is how to choose the field F to move a system from one deformation to another, when only the shapes at the endpoints are known ahead of time. We will handle this in several steps. In the first step, we describe the two shapes by fitting their multipole moments up to a certain order. Thus we calculate (cf. fig. 2)

$$Q_\nu^\lambda = \int \rho_\nu(r)\, Y_\lambda \, \mathrm{d}^3 r \qquad (\nu = \mathrm{i}, \mathrm{f}) . \tag{3.8}$$

Expanding the density to first order in the deformation parameters β_λ one can write

$$Q_\nu^\lambda = \beta_\lambda R_0 \int \frac{\mathrm{d}\rho(r)}{\mathrm{d}r} r^2 \, \mathrm{d}r . \tag{3.9}$$

The deformation parameters of the limiting shapes are given in table 1 for several cases. We assume that the path between the two shapes goes through shapes with linearly interpolated values of Q^λ. In practice we divide the path into finite segments with shapes

$$Q_n^\lambda = \frac{n}{N+1}(Q_\mathrm{f}^\lambda - Q_\mathrm{i}^\lambda) + Q_\mathrm{i}^\lambda . \tag{3.10}$$

For each small path segment n we require a field $F_n(r) = \sum_\lambda c_\lambda^n r^\lambda Y_\lambda$, that maps points on the periphery of the starting shape onto the periphery of the transformed shape. The c_λ^n's are determined iteratively starting from a guess, based on the behavior when the system is close to spherical, $c_\lambda^n \approx \Delta B_n / \lambda R_0^{\lambda-2}$. The periphery is mapped with the trial field, the new Q_n^λ is calculated, and the difference with respect to the desired value is used to make a new estimate of c_λ^n. In our calculations, we divided the path into 10 segments. The number of steps here has no physical significance; it is only necessary that the step size be small enough so that the individual displacements are small compared to a characteristic dimension of the distortions. The components of the fields c_λ for the decay $^{232}\mathrm{U} \rightarrow {}^{24}\mathrm{Ne} + {}^{208}\mathrm{Pb}$ are shown in fig. 3 for each step. We display values starting from both spherical and the deformed initial shape of the ^{232}U. Note that with a deformed uranium, very little quadrupole field is required to transform to the final shape. The transformed initial surface is in fig. 2 shown as a thin continuous curve. There where curvatures are small it matches the desired shape very well, but the neck region is not so well described by the multipole expansion with our truncation at $L = 8$. We believe that fine details in the shape evolution will occur without a cost in terms of the number of orbital jumps, provided the overall density evolution is correctly described.

Once we have obtained the field, we use the equations in appendix A to determine the distortion of the Fermi surface. The particle density outside the Fermi sphere is integrated for each step in order to get a total number of particles that moved across the Fermi surface. For example we described, $^{232}\mathrm{U} \rightarrow {}^{24}\mathrm{Ne} + {}^{208}\mathrm{Pb}$, where the number of particles that crossed the Fermi surface is 38. Recognizing that level crossings come in pairs, this means that the shape evolution can take place along a path with 19 level crossings, and a pair of particles changing orbit at each crossing.

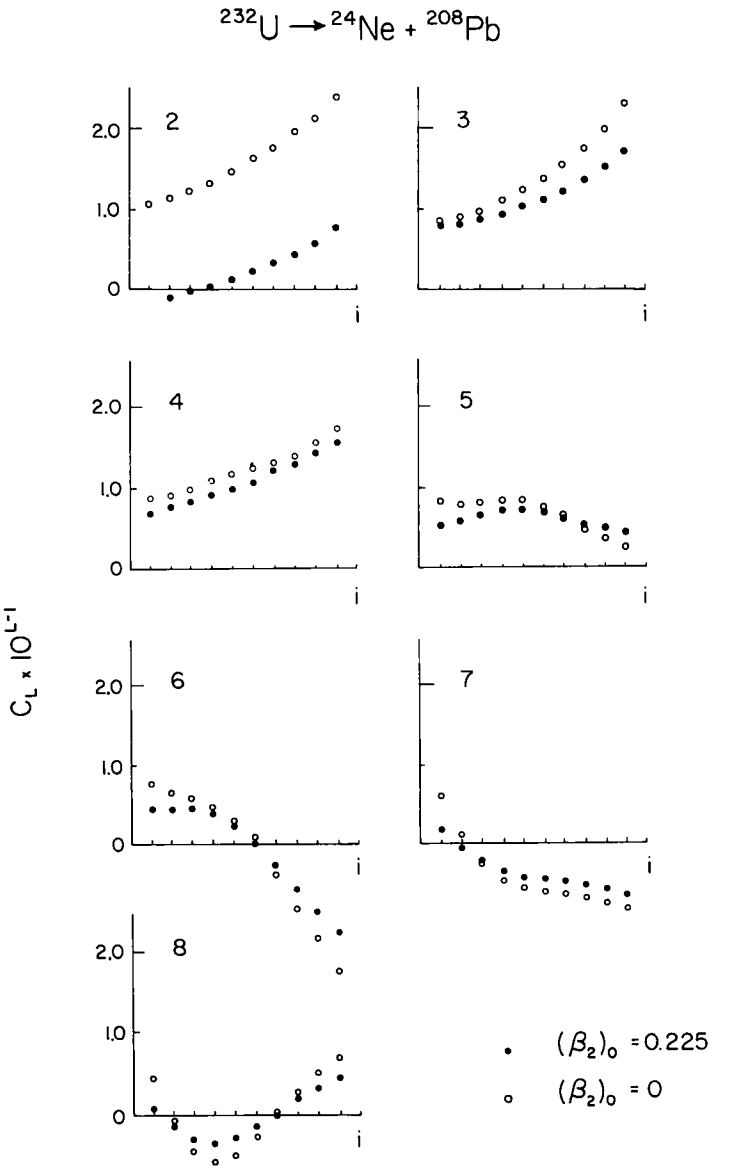

Fig. 3. The coefficient c_L of the multipole expansion (3.2) for the decay $^{232}U \rightarrow {}^{14}C + {}^{208}Pb$ (cf. fig. 2) as a function of the number of steps i. The values displayed with closed dots are associated with an initial spherical configuration of ^{232}U. Those shown with open dots correspond to a quadrupole deformed ($\beta_2 = 0.160$, $\xi = 0$) initial configuration.

TABLE 1

Deformation parameters β_λ associated with the initial and final configurations of the different exotic decay processes indicated in the first row

L	$^{222}Ra \to {}^{14}C + {}^{208}Pb$		$^{232}U \to {}^{24}Ne + {}^{208}Pb$		$^{234}U \to {}^{28}Mg + {}^{206}Pb$		$^{241}Am \to {}^{34}Si + {}^{207}Pb$	
	β_i	β_f	β_i	β_f	β_i	β_f	β_i	β_f
2	0.160 [a])	0.100	0.225 [b])	0.169	0.225 [b])	0.200	0.250 [c])	0.241
3	0	0.107	0	0.172	0	0.197	0	0.228
4	0	0.109	0	0.169	0	0.191	0	0.218
5	0	0.111	0	0.161	0	0.178	0	0.193
6	0	0.101	0	0.138	0	0.149	0	0.157
7	0	0.097	0	0.117	0	0.121	0	0.115
8	0	0.077	0	0.085	0	0.083	0	0.072

[a]) Ref. [29]).
[b]) Ref. [30]).
[c]) Ref. [31]) assuming the same β_2 as used for ^{240}Pu.

For the alpha decay, the number of level crossings comes out to about 4, corresponding to 8 particles that moved across the Fermi surface. For the heavier particles, the number of level crossings is also nearly equal to the mass number of the daughter nucleus. With a rough argument we can explain this equality as follows. The displacement field acts on the single-particle phase density without compression. When particles are moved through a surface along one direction, say the z-direction, there is a compensation shift in the distribution in p_z to preserve the phase space density. Thus we could expect that the total number of particles moved through the Fermi surface would equal the number moved through some initial spatial surface. Note that to preserve the center-of-mass position, when particles are moved outside the surface on one side, there have to be other particles moved through the surface on the other side. Thus, $2A$ particles moved through the spatial surface of the initial nuclear shape.

4. The off-diagonal interaction

We now develop a more realistic treatment of the off-diagonal interaction connecting neighboring states at different deformations. In our view, the pairing interaction is largely responsible for mixing these states. We define the pairing hamiltonian in the usual way,

$$H = -G \sum_{\nu,\nu'} a_\nu^+ a_{\bar{\nu}}^+ a_{\bar{\nu}'} a_{\nu'} . \tag{4.1}$$

Here a_ν^+ and a_ν are the fermion creation and annihilation operators, and the time reversal of the state ν is denoted $\bar{\nu}$. The sum in (4.1) is restricted to include each pair of states $(\nu, \bar{\nu})$ only once. Note that because there is no restriction on the quantum numbers; all single-particle states are connected by (4.1). This contrasts

with the behavior of single-particle fields, which have severe restrictions on allowed single-particle transitions.

The pairing interaction is important in a different way as well; pair-correlated states have greatly enhanced pair field matrix elements, compared to the pure configurations. So we will apply the results of sect. 2, not using individual configurations but, rather, pair-correlated states as the discrete wave functions on the collective path. We shall evaluate the effective v between such states starting from the BCS approximation.

Heavy nuclei are, as a rule, superfluid in their ground state. In the BCS approximation the state is described by the wave function

$$|\psi_{\mathrm{BCS}}\rangle = \prod_{\nu} (U_\nu + V_\nu a_\nu^+ a_{\bar{\nu}}^+)|\rangle . \tag{4.2}$$

The single-particle energies of the states ν are functions of the collective coordinate ξ. Very generally, one can divide these levels according to whether the energies increase or decrease with ξ. At each level crossing, a Cooper pair will be moved from an upsloping to a downsloping level under the influence of the pairing force, without being excited from the condensate. Thus, the matrix element we have to calculate is

$$\begin{aligned} v &= -G\langle\psi_-(N-n)\psi_+(n)|H_p|\psi_-(N-n+1)\psi_+(n-1)\rangle \\ &= -G\langle|\psi_-(N-n)|\sum_{\nu} a_\nu^+ a_{\bar{\nu}}^+|\psi_-(N-n+1)\rangle\langle\psi_+(n)|\sum_{\nu'} a_{\bar{\nu}'} a_{\nu'}|\psi_+(n-1)\rangle , \end{aligned} \tag{4.3}$$

where $\psi_+(n)$ and $\psi_-(N-n)$ are the wave functions associated with the upsloping and downsloping orbitals filled with n and $N-n$ pairs respectively, the total number of nucleons being $2N$.

Recognizing that the BCS wave function can be expressed as

$$|\psi_{\mathrm{BCS}}\rangle = \left(\sum_{n_2} b_{n_2}|\psi_+(n_2)\rangle\right)\left(\sum_{n_1} b'_{n_1}|\psi_-(n_1)\rangle\right), \tag{4.4}$$

where b_{n_2} and b_{n_1} are normalized amplitudes which vary smoothly with the particle number, one can approximate the matrix elements appearing in (4.3) in terms of the BCS matrix element. We write

$$\begin{aligned} \langle\psi_{\mathrm{BCS}}|\sum_{\nu} a_\nu^+ a_{\bar{\nu}}^+|\psi_{\mathrm{BCS}}\rangle = &\sum_{n_2} b_{n_2+1} b_{n_2}\langle\psi_+(n_2+1)|\sum_{\nu} a_\nu^+ a_{\bar{\nu}}^+|\psi_+(n_2)\rangle \\ &+\sum_{n_1} b'_{n_1+1} b_{n_1}\langle\psi_-(n_1+1)|\sum_{\nu} a_\nu^+ a_{\bar{\nu}}^+|\psi_-(n_1)\rangle . \end{aligned}$$

Assuming now that $\langle\psi_\pm(n\pm1)|\sum_\nu a^+ a_{\bar{\nu}}^+|\psi_\pm(n)\rangle$ are independent of n and equal to each other, and that*

$$\sum b_{n+1} b_n = \sum b'_{n+1} b'_n \approx 1 \tag{4.5}$$

* This will over estimate the matrix element, $\sin\sum_n b_{n+1}\, b_n$ will be somewhat less than one.

we obtain

$$\langle\psi_+(n+1)|\sum a_\nu^+ a_{\bar\nu}^+|\psi_+(n)\rangle \approx \langle\psi_-(n-1)|\sum a_\nu^+ a_{\bar\nu}^+|\psi_-(n)\rangle \approx \tfrac{1}{2}\langle\psi_{\rm BCS}|a_\nu^+ a_{\bar\nu}^+|\psi_{\rm BCS}\rangle . \quad (4.6)$$

Using the relation

$$\langle\psi_{\rm BCS}|\sum_\nu a_\nu^+ a_{\bar\nu}^+|\psi_{\rm BCS}\rangle = \sum_\nu U_\nu V_\nu = \frac{\Delta}{G}, \quad (4.7)$$

the matrix element v can now be written as

$$v = -\frac{G}{4}\left(\frac{\Delta}{G}\right)^2 = -\frac{\Delta^2}{4G}, \quad (4.8)$$

Δ being the pairing gap. Because in heavy nuclei, both protons and neutrons are superfluid, there will be contributions from both collectivities. We find

$$v \approx -\frac{\Delta_\nu^2 + \Delta_\pi^2}{4G}, \quad (4.9)$$

where Δ_i $(i = \pi, \nu)$ are the pairing gaps associated with each type of particles.

From eq. (2.5), the inertial mass can be written as

$$D = \hbar^2 \frac{2G}{\Delta_\nu^2 + \Delta_\pi^2}\left(\frac{{\rm d}n}{{\rm d}\xi}\right)^2 . \quad (4.10)$$

The result (4.8) is very natural, viewing the shift of a Cooper pair as a "pickup" of a pair of particles from the upsloping levels in the condensate, and a stripping onto the downsloping orbitals of the same condensate, without exciting any quasiparticle. In the BCS approximation, each of these processes is associated with an amplitude of the type of (4.7). The factor $\frac{1}{4}$ in (4.8) arises because of the four possible types of jumps of pairs between up- and downsloping levels, only one (up to down) leads to level crossings.

It is interesting to compare eq. (4.10) with the cranking inertia, as obtained in eq. (9.48) of ref. [2]), or eq. (4.47) of ref. [16]). In agreement with (4.10), the cranked inertia depends on pairing gap as $D \sim \Delta^{-2}$. The crucial role of pairing is clear from this functional dependence. The larger the pairing gap, the smaller the inertia for collective motion, i.e. the easier it is for the system to move collectively. This is just a physical statement of superfluidity.

The coefficient of Δ^{-2} is different in our approach and the cranking model. In our model the coefficient depends on G, the pairing interaction, while in the cranking model it depends only on the slope of single-particle energies with respect to deformation. The validity of the two approaches has been examined in various models. In the model discussed in ref. [5]), the present approach was found to be accurate while the cranking model could be quite misleading, depending on the choice of the cranking field. In another model discussed in ref. [17]), the cranking

model was found to be correct in the adiabatic limit, as expected. This limit requires that the frequency of the motion satisfy $\omega \ll \Delta$. In the opposite limit, $\omega \gg \Delta$, our expression (4.10) becomes more accurate. Perhaps coincidentally, the two inertias agree in practice to about a factor of two. We conclude from this discussion that the theoretical inertia is probably uncertain to about a factor of two, and thus we cannot hope for high accuracy in the predictions of the theory.

In the systematic study we make in the next sections, we adopt for the pairing strength [18])

$$G = \frac{25}{A}\,\mathrm{MeV}.$$

For Δ, we believe it is best to take a systematic average value rather than an empirical value that would be valid only at one fixed shape. We adopt the usual systematic formula [19]),

$$\Delta = \frac{12}{\sqrt{A}}\,\mathrm{MeV}.$$

With these prescriptions, the effective interaction connecting neighboring shapes is given by

$$v \approx -2.9\ \mathrm{MeV}.$$

Note that the A-dependence has dropped out completely.

This magnitude of the off-diagonal interaction is consistent even with what is required in light nuclei such as ^{16}O or ^{40}Ca to understand the mixing of multiparticle-multihole states [20]).

5. Explicit treatment of protons and neutrons

Because the pairing gap and pairing coupling constants, as well as the number of level crossings can be quite different for protons and neutrons, it is in some cases necessary to treat both degrees of freedom explicitly.

We start defining a center-of-mass and relative motion collective coordinates

$$z = z_\pi - z_\nu, \tag{5.1}$$

$$Z = \frac{D_\pi z_\pi + D_\nu z_\nu}{D_\pi + D_\nu}, \tag{5.2}$$

$$D = D_\pi + D_\nu, \tag{5.3}$$

where z_i and D_i $(i = \pi, \nu)$ are the collective coordinates and the inertial masses associated with particles of type i.

The collective kinetic energy

$$T = -\frac{\hbar^2}{2D_\pi}\frac{\mathrm{d}^2}{\mathrm{d}z_\pi^2} - \frac{\hbar^2}{2D_\nu}\frac{\mathrm{d}^2}{\mathrm{d}z_\nu^2} \tag{5.4}$$

expressed in terms of the variables (5.1) and (5.2) becomes

$$T = T_{\text{c.m.}} + T_{\text{rel}}, \tag{5.5}$$

where

$$T_{\text{c.m.}} = -\frac{\hbar^2}{2D}\frac{\mathrm{d}^2}{\mathrm{d}Z^2}, \tag{5.6}$$

$$T_{\text{rel}} = -\frac{\hbar^2}{2d}\frac{\mathrm{d}^2}{\mathrm{d}z^2}. \tag{5.7}$$

The quantity

$$d = \frac{D_\pi D_\nu}{D_\pi + D_\nu}, \tag{5.8}$$

is the reduced mass of the system.

Contrary to standard quantal problems, here it is the center-of-mass motion which is interesting, the relative degree of freedom being essentially trivial. Because of the very strong repulsive isovector potential V_1, it is energetically very unfavorable to deform the neutron- and proton-densities separately. Collective isovector oscillations all lie at high frequency. Thus the motion in the z-coordinate will adiabatically follow the Z-coordinate for the large-amplitude processes we consider here.

One can thus identify Z with the collective coordinate ξ used in previous sections, or if protons and neutrons are treated explicitly $Z_\nu \to \xi_\nu$ and $Z_\pi \to \xi_\pi$.

Different approximations to the corresponding equations can be used in the case where

$$\Delta_\pi \approx \Delta_\nu \approx \Delta; \qquad G_\pi \approx G_\nu \approx G, \qquad \frac{\mathrm{d}n}{\mathrm{d}z_\pi} \approx \frac{\mathrm{d}n}{\mathrm{d}z_\nu}. \tag{5.9}$$

In this case $D_\nu \approx D_\pi$ and

$$\frac{\mathrm{d}n}{\mathrm{d}z_i} = \frac{\mathrm{d}n}{\mathrm{d}Z}\frac{\mathrm{d}Z}{\mathrm{d}z_i} = \frac{1}{2}\frac{\mathrm{d}n}{\mathrm{d}Z}. \tag{5.10}$$

Consequently

$$D \approx \hbar^2 \frac{G}{\Delta^2}\left(\frac{\mathrm{d}n}{\mathrm{d}Z}\right)^2 \approx \hbar^2 \frac{2G}{\Delta_\nu^2 + \Delta_\pi^2}\left(\frac{\mathrm{d}n}{\mathrm{d}Z}\right)^2 \approx -\frac{\hbar^2}{2v}\left(\frac{\mathrm{d}n}{\mathrm{d}Z}\right)^2, \tag{5.11}$$

as obtained before in eq. (4.10).

6. Connection to the external region

Having specified the dynamics from the parent shape to the touching daughter shapes, we must still propagate the nuclei under the external Coulomb barrier. In

this region the wave function is described by the relative coordinate between the two daughter nuclei, multiplied by the internal wave functions of the daughters. On the other hand, up to the touching point the wave function is expressed in terms of single-particle orbitals, without well-defined positions for the daughter nuclei. There are two ways these representations can be connected to make a theory of the decay rate, using the Gamow formula or Fermi's Golden Rule.

In the Gamow theory, the rate is expressed as

$$\lambda = SfT, \tag{6.1}$$

where S is the probability of forming the daughter nuclei, f is a barrier assault frequency, and T is the transmission factor of the barrier. If we were to use this formula, S would be calculated as $S = a_n^2$. Calculating combination fT is more problematic, because the formula requires the external potential to produce a resonance at the appropriate energy and spatial position. In general the external potentials do not produce resonances whose wave functions peak around the touching distance R_0.

For this reason we calculate the decay rate by the Golden Rule, which does not make any demands on the final-state wave function. The formula requires the matrix element of the hamiltonian between an initial state and a final state. We take the initial state to be the eigenfunction of the hamiltonian discussed in sects. 2 and 4, omitting however the final configuration of touching spheres. The final wave function is the continuum wave function of the daughter nuclei treated as particles, in which the relative wave function is calculated by solving the Schrödinger equation. The matrix element connecting these is v, the matrix element to the touching daughter configuration, multiplied by the probability of that configuration in the continuum final state. The formula is

$$\lambda = 2\pi (a_{n-1}^0)^2 v^2 \frac{\mathrm{d}N}{\mathrm{d}E} \langle \phi_n | \psi_E \rangle^2 . \tag{6.2}$$

Here a_{n-1}^0 is the amplitude of the $(n-1)$ configuration in the eigenstate of the internal hamiltonian, obtained by diagonalizing eq. (2.1). The continuum wave function ψ_E will be calculated from a one-body potential as mentioned above.

To take the overlap we have to write the ϕ_n configuration as a product of two internal wave functions and a wave function describing the relative motion. In light nuclei, this cluster decomposition can be carried out with harmonic oscillator wave functions and yields some harmonic-oscillator function for the relative coordinate. However, most of the wave function in the inside is unphysical because the wave function is antisymmetrized overall. We thus consider that a reasonable approximation to the cluster wave function would be just the first peak in the harmonic-oscillator relative wave function. For the accuracy of the calculations we are doing here, we consider it adequate to make a further approximation, taking the wave function as a gaussian centered at the separation distance R_t of the two nuclei in the touching

configuration. We take the touching distance as $R_t = 1.2\,(A^{1/3} + a^{1/3})$. The appropriate gaussian wave function would have a size parameter which is the same as the harmonic-oscillator wave function of the lighter daughter nucleus, $\phi_n \sim e^{-\nu(r-R_t)^2/2}\psi_a\psi_A$, with $\nu = (45a^{-1/3} - 25a^{-2/3})a/41.5\,\mathrm{fm}^{-2}$. In keeping with this ansatz, we obtain

$$\langle \phi_n | \psi_E \rangle \approx \left(\frac{\pi}{\nu}\right)^{1/4} \sqrt{2}\psi_E(R)\,.$$

The density of final states $\mathrm{d}N/\mathrm{d}E$ in eq. (6.2) is connected with the normalization of the continuum wave function. We use the asymptotic normalization $\chi_E(r) \to Y_{LM}(\Omega)\sin(kr + \delta)/r$ which implies $\mathrm{d}N/\mathrm{d}E = 2\mu/\pi k$.

The continuum wave function ψ_E should be calculated from a proximity potential consistent with the known heavy-ion interaction systematics, since the particles are in the external region. We have used a potential with the nuclear part taken from eqs. (III.1.40)-(III.1.43) of ref. [27]), giving

$$V(r) = \frac{-V_0}{1 + e^{(r-R_0)/a}} + \frac{Z_a Z_A e^2}{r}\,, \tag{6.3}$$

where

$$V_0 = 16\pi\gamma\bar{R}_{aA}a\,.$$

The surface tension γ is given by

$$\gamma = 0.95\left[1 - 1.8\left(\frac{N_a - Z_a}{A_a}\right)\left(\frac{N_A - Z_A}{A_A}\right)\right] \mathrm{MeV}\cdot\mathrm{fm}^{-2}$$

while the reduced radius

$$\bar{R}_{aA} = \frac{R_a R_A}{R_a + R_A}$$

is defined in terms of the radii $R_i = 1.233\,A_i^{1/3} - 0.98\,A_i^{-1/3}$ fm. The diffusivity parameter and well radius in the potential are given by $a = 0.63$ fm and $R = R_a + R_A + 0.29$ fm. We integrate the Schrödinger equation in an outward direction, starting the wave function zero at 1-2 fm inside R. The wave function of course grows exponentially in the forbidden region and turns into an oscillating function in the outer allowed region. We integrate to the second peak in the allowed region, which occurs at a radius R'. Then the normalized wave function is determined as

$$\psi\left(\frac{\mathrm{d}n}{\mathrm{d}E}\right)^{1/2} \approx \frac{u(R)}{u(R')}\left(\frac{1}{\pi}\sqrt{\frac{2\mu}{E - V(R)}}\right)^{1/2}$$

where $V(R')$ is the potential at R' and μ is the reduced mass of the $a + A$ system. An example of a wave function is shown in fig. 4.

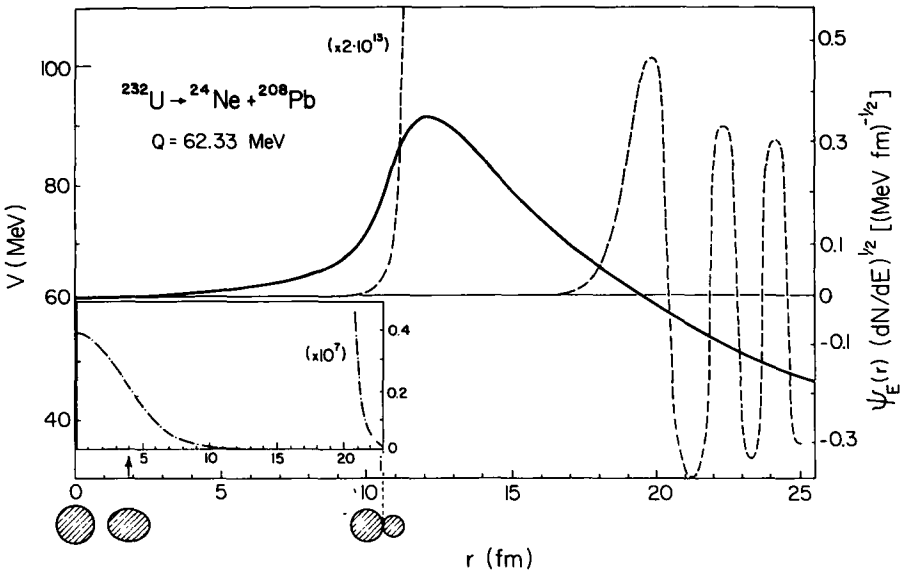

Fig. 4. The potential energy of the system $^{232}U \rightarrow {}^{24}Ne + {}^{208}Pb$ is shown with a continuous line. The amplitudes a_i^0 as a function of the step i are displayed in the inset with a dashed-dotted curve. The product of the continuous wave function and of the square root of the density of states is plotted as a function of the relative distance with a dashed curve.

7. Results and discussion

The diagonal interaction for the hamiltonian in the internal region is still to be specified. In principle this requires Hartree-Fock or Strutinsky calculations, and the result would be a potential energy surface with shell fluctuations. We shall however assume, as others do, that the shell fluctuations are not too violent and the potential may be smoothly interpolated between the endpoints. We assume the potential energy varies quadratically about the minimum point, $Q-2v$ (cf. e.g. eq. (2.5)), and passes through the energy of the touching configuration as determined above with the heavy-ion potential. An example is displayed in fig. 4.

The results of the model applied to representative alpha decays and the heavy-particle radioactivity are shown in tables 2 and 3.

The effective preformation factors $(a_{n-1}^0)^2$ are of the order of a few percent for alpha radioactivity. For heavy-particle radioactivity this quantity is very small, ranging from 10^{-10} to 10^{-20}. The nucleus can fluctuate to make the alpha particle on the surface relatively easily, but not so to produce a C- or a Ne-particle. The amplitudes which we have calculated with the formalism discussed above, a_i^0, can be parameterized according to $a_i^0 \sim \exp[-(i/n)^2 n(\Delta E/v)^{1/2}]$, where $\Delta E = U_c + U_N - Q + 2v$ is the energy needed for the system to get to the emission point.

The theoretical α decay rates are generally within an order of magnitude of the experimental. An exception is ^{223}Ra, which is predicted too fast by a factor of 22.

TABLE 2

The calculated decay constants for α-decay from the parent nucleus listed in column 1 are compared with the experimental data in columns 6 and 7. In column 2, the Q-value of the decay is given. In column 3 we give the value of the constant $\frac{1}{2}C$ of the harmonic oscillator potential $V(\xi)=\frac{1}{2}c\xi^2$ between the initial configuration ($\xi=0$), touching sphere configuration ($\xi=1$). The value of the pairing matrix element between neighbor configurations used in the calculation is the standard one $v_{\text{int}}=2.9$ MeV. In columns 4 and 5 we give respectively the amplitude of the internal wave function at the pre-formation point and the amplitude of the Coulomb wave function at the formation point. We have calculated the number of steps n_{step} needed to reach the final configuration using the phase-space method, obtaining in all cases $n_{\text{step}}\approx 4$. The density of states in the continuum is $\rho=0.14\ \text{MeV}^{-1}\ \text{fm}^{-1}$

Decay	Q (MeV)	$\frac{1}{2}c$ (MeV)	a_{n-1}	$\Psi(R)(\mathrm{d}n/\mathrm{d}E)^{1/2}$ $(\text{MeV}\cdot\text{fm})^{-1/2}$	$\lambda(\text{s}^{-1})$	$\lambda_{\text{exp}}(\text{s}^{-1})$
$^{223}\text{Ra}\rightarrow\alpha$	5.980	1.49	0.203	4.1×10^{-14}	1.6×10^{-5}	7.0×10^{-7}
$^{224}\text{Ra}\rightarrow\alpha$	5.789	1.64	0.198	1.4×10^{-14}	1.7×10^{-6}	2.2×10^{-6}
$^{226}\text{Ra}\rightarrow\alpha$	4.871	2.47	0.174	3.1×10^{-17}	6.5×10^{-12}	1.4×10^{-11}
$^{231}\text{Pa}\rightarrow\alpha$	5.148	2.92	0.162	4.0×10^{-17}	9.0×10^{-12}	6.7×10^{-13}
$^{232}\text{U}\rightarrow\alpha$	5.413	2.93	0.162	1.4×10^{-16}	1.1×10^{-11}	3.2×10^{-10}
$^{233}\text{U}\rightarrow\alpha$	4.909	3.39	0.152	3.5×10^{-18}	6.2×10^{-14}	1.4×10^{-13}
$^{234}\text{U}\rightarrow\alpha$	4.860	3.39	0.152	2.4×10^{-16}	2.9×10^{-14}	9.0×10^{-14}
$^{241}\text{Am}\rightarrow\alpha$	5.638	3.25	0.155	1.3×10^{-17}	8.2×10^{-11}	5.1×10^{-11}

On the average, the logarithm of transition rates differs from the experimental by +0.1, showing that the model would not be much improved by refining its parameters.

For the heavy-particle radioactivity, the predicted rates tend to be too fast for ^{14}C decays and too slow for the heaviest emitted nuclei, such as ^{28}Mg and ^{32}Si. In view of the extreme sensitivity of the rates to the inertial parameter, this is perhaps to be expected. However, we find the situation satisfactory that the overall systematics of the rates are reproduced by a microscopic model with no adjustable parameters.

We now briefly discuss the relationship to other theories of heavy-particle radioactivity. There are a number of macroscopic models [21-23]), in which no connection is made to the underlying nucleon structure of the wave function. A collective coordinate is postulated for an internal degree of freedom which smoothly joins onto the separation coordinate between the final state daughter nuclei. In refs. [22,24]), the inertia is assumed to have the classical liquid drop value. In view of the fact that our inertia reproduces the overall systematics, we find it surprising that the calculations with a classical inertia do not consistently overpredict the transition rates. It is known from the dynamics of quadrupolar motion that the microscopic inertia is an order of magnitude larger than the liquid drop inertia. One would anticipate that to be the case also for the more complex motions described here.

Besides our own model, there was another study based on nucleon wave functions reported in ref. [24]). In this microscopic theory, the authors calculate a spectroscopic factor for the cluster formation simply by projecting the daughter configuration out of the initial parent wave function. Thus, all the fluctuations to the final shape are

TABLE 3

Lifetimes associated with exotic decay processes, as indicated in the first column. The Q-value of the decay is given in the second column. The spring constant describing the internal part of the potential in the harmonic approximation is listed in the third column. Columns 4 and 5 give the number of steps and the amplitudes a^0_{n-1} for the heavy particle to be formed. The continuum wave function is listed in column 6. In the last two columns the calculated and experimental lifetimes are given. See ref. [29]) for citations of the experimental data.

Decay	Q (MeV)	$\frac{1}{2}c$	n	a^0_{n-1}	$\psi_E(R)(\mathrm{d}n/\mathrm{d}E)^{1/2}$ $(\mathrm{MeV}\cdot\mathrm{fm})^{-1/2}$	λ (s^{-1})	log $t_{1/2}$ (s)	
							theory	exp.
^{221}Fr (^{14}C)	31.28	6.34	12	0.29E−3	−0.15E−14	0.24E−13	13.5	> 15.77
^{221}Ra (^{14}C)	32.39	6.02	12	0.34E−3	−0.56E−14	0.47E−12	11.7	> 14.35
^{222}Ra (^{14}C)	33.05	5.29	12	0.51E−3	−0.23E−13	0.19E−10	10.6	11.02 (0.06)
^{223}Ra (^{14}C)	31.85	6.41	12	0.28E−3	−0.20E−14	0.39E−13	13.2	15.2 (0.05)
^{224}Ra (^{14}C)	30.53	7.65	12	0.15E−3	−0.11E−15	0.35E−16	16.3	15.9 (0.12)
^{225}Ac (^{14}C)	30.47	8.43	12	0.10E−3	−0.33E−16	0.15E−17	17.7	> 18.34
^{226}Ra (^{14}C)	28.21	9.82	12	0.56E−4	−0.40E−18	0.68E−22	22.0	21.33 (0.2)
^{230}Th (^{24}Ne)	57.78	12.71	19	0.19E−7	−0.11E−16	0.43E−26	26.2	24.64 (0.07)
^{232}Th (^{26}Ne)	55.97	13.47	21	0.16E−8	−0.22E−18	0.13E−31	31.7	> 27.94
^{231}Pa (^{24}Ne)	60.42	11.22	19	0.46E−7	−0.22E−15	0.11E−22	22.8	23.38 (0.08)
^{232}U (^{24}Ne)	62.33	10.48	19	0.75E−7	−0.11E−14	0.78E−21	21.0	21.06 (0.1)
^{233}U (^{24}Ne)	60.50	12.17	19	0.26E−7	−0.68E−16	0.33E−24	24.3	24.82 (0.15)
^{234}U (^{24}Ne)	58.84	13.72	19	0.10E−7	−0.45E−17	0.24E−27	27.5	25.25 (0.05)
^{234}U (^{26}Ne)	59.47	12.19	21	0.37E−8	−0.66E−17	0.61E−28	28.0	
^{234}U (^{28}Mg)	74.13	13.63	23	0.19E−9	−0.11E−15	0.46E−28	28.2	25.75 (0.06)
^{237}Np (^{30}Mg)	75.02	13.06	24	0.11E−9	−0.67E−16	0.49E−29	29.1	> 27.27
^{238}Pu (^{30}Mg)	77.03	12.38	24	0.18E−9	−0.28E−15	0.25E−27	27.5	25.7 (0.25)
^{238}Pu (^{28}Mg)	75.93	14.31	23	0.12E−9	−0.89E−16	0.11E−28	28.8	
^{238}Pu (^{32}Si)	91.21	13.69	26	0.87E−11	−0.15E−14	0.17E−28	28.6	25.3 (0.16)
^{241}Am (^{34}Si)	93.84	11.60	27	0.19E−10	−0.85E−14	0.25E−26	26.4	> 25.3; > 24.2

already contained in the ground-state wave function. It seems surprising that a large enough spectroscopic factor is obtained in this way. At the level of Hartree-Fock wave functions, conservation of the K quantum number makes the spectroscopic factor identically zero in many cases. However, the wave functions used in ref. [24]) include pairing, and so some of the physics on which we rely is also implicit in their treatment. Also, their joining point is at a smaller separation than the touching daughter configuration, so the required spectroscopic factor is not as large as in our treatment. These authors further developed a systematics [25]) with the spectroscopic factor proportional to a power of the number of particles in the daughter, $S(A) = S(\alpha)^{(A-1)/3}$. In our treatment, the probability is exponential in n and $n \approx A - 1$ suggests a similar scaling. However, the potential function varies from case to case so we did not find a universal scaling behavior.

Finally, we mention the work of Buck and Merchant [26]), who use a cluster description with unit spectroscopic factor and get good agreement for both α and heavy-particle radioactivity. It is only possible to have $S = 1$ with a more repulsive potential in the external region; their analytic potential does not have the characteristics just outside the touching point required to describe heavy ion fusion and scattering data. These authors also use a spin-dependent prefactor in their (fT) formula for which we cannot find a justification.

One last point relates to the pairing, which is seen to be an essential part of microscopic theory. Since pairing is reduced by odd nucleons, the decay rates should show a pronounced odd-even effect. While the data show the effect in a qualitative way, the magnitude is smaller than would be expected for a rate depending exponentially on the pairing gap.

G.B. acknowledges support by the National Science Foundation under grant PHY 87-14432.

Appendix

In order to characterize the shape of the nuclear surface, one can express the radius as a function of the angle by

$$R(\theta) = R\left(1 + \sum_L \beta_L Y_L(\theta)\right), \tag{A.1}$$

where R is the radius of the undeformed sphere and $Y_L(\theta)$ is the spherical harmonic $Y_{LM}(\theta)$ with $M = 0$. (We only consider axially symmetric deformations here.)

Then the density distribution of the deformed nucleus is

$$\rho_\beta(r, \theta) \approx \rho(r) - \sum_L \beta_L R \frac{\partial \rho(r)}{\partial r} Y_L(\theta). \tag{A.2}$$

Multiplying this equation by $Y_L(\theta)$ and integrating, one obtains

$$\beta_L = -\frac{2\pi \int \rho_\beta(r,\theta)\, Y_L(\theta)\, \mathrm{d}\theta\, \mathrm{d}r}{R \int (\partial_\rho/\partial r)\, \mathrm{d}r} = \frac{2\pi \int \rho_\beta(r,\theta)\, Y_L(\theta)\, \mathrm{d}\theta\, \mathrm{d}r}{R\rho(r=0)}. \tag{A.3}$$

Note that while (A.2) is valid only for small deformations, (A.3) is valid in general. Calling $[\beta_L^0]$ the set of deformation parameters of the two touching spheres configuration, one can characterize an intermediate configuration $[\beta_L]$ using a collective coordinate ξ, defined as

$$\beta_L = \xi \beta_L^0, \qquad 0 \leqslant \xi \leqslant 1, \tag{A.4}$$

which means that we consider a one-dimensional problem.

The change from one value of ξ to $\xi + \mathrm{d}\xi$ implies the flow of the Fermi liquid, that we characterize by the field of displacements $\boldsymbol{u}(\boldsymbol{r}, \xi)\, \mathrm{d}\xi$. We assume that there is no compression of the liquid, that is, $\nabla \cdot \boldsymbol{u} = 0$; then the field of displacements can be written

$$\boldsymbol{u}(\boldsymbol{r}, \xi) = \sum_L c_L(\xi) \nabla [r^L Y_L(\theta)]. \tag{A.5}$$

In the following the dependence on ξ will be understood, and not written explicitly.

The c_L parameters can be determined from the β_L requiring (see fig. 3)

$$R_\xi(\theta) \cos\theta + u_z(R_\xi(\theta), \theta)\, \mathrm{d}\xi = R_{\xi+\mathrm{d}\xi}(\theta') \cos\theta', \tag{A.6a}$$

$$R_\xi(\theta) \sin\theta + u_x(R_\xi(\theta), \theta)\, \mathrm{d}\xi = R_{\xi+\mathrm{d}\xi}(\theta') \sin\theta', \tag{A.6b}$$

where θ' is given by

$$\sin\theta' = \frac{R_\xi(\theta) \sin\theta + u_x(R_\xi(\theta), \theta)\, \mathrm{d}\xi}{[R_\xi^2(\theta) + u^2(R_\xi(\theta), \theta)\, \mathrm{d}\xi + 2\boldsymbol{u}(R_\xi(\theta), \theta) \cdot R_\xi(\theta)\, \mathrm{d}\xi]^{1/2}}$$

u_x and u_z can be related to the c_L parameters noting that

$$u_x = u_\theta \cos\theta + u_r \sin\theta, \qquad u_z = -u_\theta \sin\theta + u_r \cos\theta,$$

where

$$u_r(r,\theta) = \sum_L c_L L r^{L-1} Y_L(\theta), \qquad u_\theta(r,\theta) = \sum_L c_L r^{L-1} \frac{\mathrm{d}Y_L(\theta)}{\mathrm{d}\theta}.$$

Writing the same equations at different points on the surface one obtains a system of equations that is linear in the c_L, except for the dependence of θ' in c_L. This system can be solved following an iterative procedure and using the least square method.

Due to deformation, the kinetic energy of the nucleons increases as long as there is no change in the single-particle configuration. The increase in the kinetic energy is due to a deformation of the Fermi surface, which is given by the transformation [13])

$$\boldsymbol{p} \to (1 + \mathrm{d}\xi(\nabla \times \boldsymbol{u}))\boldsymbol{p}, \tag{A.7}$$

where $\nabla \times \boldsymbol{u}$ is a tensor that can be written as

$$\nabla \otimes \boldsymbol{u} = \sum_L c_L (\nabla \otimes \boldsymbol{u})_L$$

with

$$(\nabla \otimes \boldsymbol{u})_L = \nabla \otimes (\nabla r^L Y_L(\theta))$$

The increase in kinetic energy continues until a level crossing occurs, that is, until there is a change in the quasiparticle configuration. This, on average, happens each time the volume of the phase space outside the Fermi sphere is equal to the phase space occupied by the particles jumping from one orbital to another at the level crossing. With the change of configuration the Fermi surface becomes again spherical, diminishing in this way the kinetic energy and leading to a new minimum in energy, which we can identify with a locally stable HF configuration.

In order to calculate the number of crossings along the trajectory in deformation space towards the scission point, one can simply count the number of times the phase space volume outside the Fermi sphere reaches the value corresponding to two particles. We have performed this procedure dividing the path into 10 steps, and calculating at each step how much of the phase space volume (V_{ex}) is outside the Fermi sphere. We consider that at each of these steps the initial Fermi surface is spherical, using the expression

$$V_{\mathrm{ex}} = \int_0^{2\pi} \mathrm{d}\phi \int_0^{\pi} \sin\theta \, \mathrm{d}\theta \int_0^{\infty} r^2 \rho(r) \, \mathrm{d}r \times \int_0^{2\pi} \mathrm{d}\phi_p \int_{L(\theta, r, \phi_p)} \sin\theta_p \, \mathrm{d}\theta_p \int_{p_{\mathrm{F}}}^{p_{\mathrm{s}}(\theta, r, \theta_p, \phi_p)} p^2 \, \mathrm{d}p, \tag{A.8}$$

where $p_{\mathrm{s}}(\theta, r, \theta_p, \phi_p)$ is the limiting momentum of the Fermi surface for a given direction in momentum space. The integration over θ_p is performed in the domain $L(\theta, r, \phi_p)$ corresponding to the points that satisfy the condition

$$p_{\mathrm{s}}(\theta, r, \theta_p, \phi_p) > p_{\mathrm{F}}.$$

In the expression (A.8) for V_{ex} the integration over ϕ gives immediately 2π due to the axial symmetry in spatial deformation. The integration over p is also immediate since the limits of integration have been already calculated as explained above. For the integration over the momentum angular coordinates θ_p and ϕ_p we use as coordinate system the principal axes of $\nabla \times \boldsymbol{u}$. Then the integration over the momentum coordinate is just the calculation of the volume of the paraboloid, that is not

within a sphere of radius p_F. The paraboloid is not exactly axially symmetric, but in order to simplify the integration over ψ_p we approximate it with another paraboloid, axially symmetric and with the same volume. In this way we end up with a three-dimensional integral that we calculate numerically [cf. eq. (3.5a, b)].

References

1) P. Bonche, P.H. Heenen, H. Flocard, and D. Vautherin, Phys. Lett. **B175** (1986) 387
2) M. Brack, J. Damgaard, A. Jensen, H. Pauli, V. Strutinsky and C. Wong, Rev. Mod. Phys. **44** (1972) 320
3) P. Möller and J.R. Nix, Nucl. Phys. **A361** (1981) 117
4) W. Nazarewicz, G.A. Leander and J. Dudek, Nucl. Phys. **A467** (1987) 437
5) P. Arve, G. Bertsch, J. Negele and G. Puddu, Phys. Rev. **C36** (1987) 2018
6) J. Negele, MIT preprint CTP#1723 (1989)
7) J. Negele, Rev. Mod. Phys. **54** (1982) 913
8) F. Barranco, R.A. Broglia and G.F. Bertsch, Phys. Rev. Lett. **60** (1988) 507
9) F. Barranco, E. Vigezzi, R.A. Broglia and G.F. Bertsch, Phys. Rev. **C38** (1988) 1523
10) B. Herskind, B. Lauritzen, K. Schiffer, R.A. Broglia, F. Barranco, M. Gallardo, J. Dudek and E. Vigezzi, Phys. Rev. Lett. **59** (1987) 2416
11) T. Bengtsson *et al.*, Phys. Rev. Lett. **62** (1989) 2448
12) D.L. Hill and J.A. Wheeler, Phys. Rev. **89** (1953) 1102
13) G.F. Bertsch, Phys. Lett. **B95** (1980) 157
14) G.F. Bertsch in Proc. of the CIV "E. Fermi" International School of Physics, Frontiers and borderlines in many-particle physics, ed. R.A. Broglia and J.R. Schrieffer (North-Holland, Amsterdam, 1988) p. 41
15) D. Zheng, D. Berdichevsky and L. Zamick, Phys. Rev. Lett. **60** (1988) 2262
16) L. Wilets, Theories of nuclear fission, (Oxford Univ. Press, 1964)
17) P. Avre and G. Bertsch, Phys. Lett. **B215** (1988) 1
18) R.A. Broglia, D.R. Bes and B.S. Nilsson, Phys. Lett. **B50** (1974) 213
19) A. Bohr and B.R. Mottelson, Nuclear structure, vol. II (Benjamin, Reading, 1985)
20) G.E. Brown and A.M. Green, Nucl. Phys. **75** (1965) 401;
W.J. Gerace and A.M. Green, Nucl. Phys. **A93** (1967) 110
21) D.N. Poenaru *et al.*, Phys. Rev. **C32** (1985) 572
22) Y.J. Shi and W. Swiatecki, Nucl. Phys. **A438** (1985) 450; Phys. Rev. Lett. **54** (1985) 300
23) G. Pik-Pichak, Sov. J. Nucl. Phys. **44** (1986) 923
24) R. Blendowski, T. Fliessbach and H. Walliser, Nucl. Phys. **A464** (1987) 75
25) R. Blendowski and H. Walliser, Phys. Rev. Lett. **61** (1988) 1930
26) B. Buck and A.C. Merchant, J. of Phys. **G15** (1989) 615
27) R.A. Broglia and A. Winther, Heavy ion reactions, vol. I (Benjamin, Reading, 1981)
28) P.B. Price, Ann. Rev. Nucl. Part. Sci. **39** (1989), to be published
29) C.M. Lederer *et al.*, Table of isotopes. 7th edition (Wiley, New York, 1978) p. 1384
30) H. Ton *et al.*, Nucl. Phys. **A155** (1970) 235
31) C.E. Bernis Jr. *et al.* Phys. Rev. **C8** (1973) 196